

# Pulse-regulated single-photon generation via quantum interference in a $\chi^{(2)}$ nonlinear nanocavity

YUYI YAN<sup>1</sup>, YANBEI CHENG<sup>1</sup>, SHENGGUO GUAN<sup>1</sup>, DANYING YU<sup>1</sup>, AND ZHENGLU DUAN<sup>1,\*</sup>

<sup>1</sup>College of Physics and Communication Electronics, Jiangxi Normal University, Nanchang, 330022, China

\*Corresponding author: duanzhenglu@jxnu.edu.cn

Compiled October 11, 2018

**A scalable on-chip single-photon source at telecommunications wavelengths is an essential component of quantum communication networks. In this work, we numerically construct a pulse-regulated single-photon source based on an optical parametric amplifier in a nanocavity. Under the condition of pulsed excitation, we study the photon statistics of the source using the Monte Carlo wave-function method. The results show that there exists an optimum excitation pulse width for generating high-purity single photons, while the source brightness increases monotonically with increasing excitation pulse width. More importantly, our system can be operated resonantly and we show that in this case the oscillations in  $g^{(2)}(0)$  is completely suppressed.**

© 2018 Optical Society of America

<http://dx.doi.org/10.1364/ao.XX.XXXXXX>

With the rapid development of quantum technologies, quantum information processing (QIP) has undergone a transition from a scientific research field to a research-usable technology, with two main practical applications, namely, quantum communication [1] and quantum computation [2]. As reliable information carriers, single photons are indispensable in applications of photon-based QIP [3]. In particular, a high-quality single-photon source in telecommunications bands would enable access to fiber-based quantum communication with low dispersion and low loss [4].

One possible method for generating single photons is to use the quantum-interference-induced photon antibunching effect, also known as the unconventional photon blockade effect [5, 6]. This photon preparation method requires only very weak nonlinearity, in contrast to the strong nonlinearity required to induce conventional photon blockade [7]. Quantum-interference-induced photon antibunching has been proposed theoretically [8] and realized experimentally [9, 10] in various systems, such as coupled cavities, atomic-optomechanical hybrid systems and superconducting circuits. Quantum-interference-induced photon antibunching has also been observed in a degenerate

optical parametric amplifier [11, 12]. As pointed out in Ref. [11], the physical basis of this mechanism is that destructive interference between a two-photon transition and a one-photon transition leads to a low or even vanishing probability of the two-photon state. Since this state is similar to a coherent field without the two-photon term, it has been termed a “modified coherent state” [13]. More recently, researchers have pointed out [14] and further clarified [8] that this state actually is an optimized Gaussian squeezed state. Such states have been used as single-photon sources [12] and in quantum cryptography [15].

In a degenerate parametric down-conversion process in a bulk  $\chi^{(2)}$  crystal or waveguide, strong second-harmonic light can efficiently generate fundamental-wave photons under the condition of phase matching. However, nonlinear interactions between light fields and materials are usually weak, and hence high light intensities and long interaction times are required to achieve high conversion efficiency. Fortunately, a high-quality double-resonance optical cavity can trap both second-harmonic and fundamental-mode light for a longer time and enhance their effective intensities, resulting in greatly enhanced nonlinear conversion efficiency [16]. Therefore, devices in which parametric processes occur inside a microcavity or nanocavity have been proposed and fabricated, such as photonic crystal cavities [17] and micro-ring/disk assemblies [18, 19], thereby extending traditional bulk optics to the micro- and nanoscales.

Thanks to the availability of nanofabrication technology, it has been possible to develop an on-chip single-photon source with strong antibunching with the advantages of compactness and scalability [20]. However, the challenge remains of preparing an on-demand integrable single-photon source at telecommunications wavelengths with high purity and efficiency [21]. To date, most studies of quantum-interference-induced photon antibunching have dealt with the case of continuous-wave (CW) driving and much less work has been done on pulsed driving [22], which is required by on-demand photon sources.

Motivated by the above considerations, in this work, we investigate single-photon generation under pulsed excitation at telecommunications wavelengths via quantum interference in a nanocavity made of weak  $\chi^{(2)}$  nonlinear material. For instance, III–V semiconductors, which have low losses in the near-infrared region, are potential candidates for such  $\chi^{(2)}$  nonlinear materials. Compared to those single photon sources based on strong  $\chi^{(2)}$  nonlinearity [23] or coupled  $\chi^{(2)}$  nonlinear nanocav-

ities [24], the scheme considered in the work merely requires a single double-resonance nanocavity with weak  $\chi^{(2)}$  nonlinearity, which is easier to realize in real experiments. Using the Monte Carlo wave-function method, we simulate the photon emission process and study the photon statistics. We find that there is an optimum pulse width for achieving high purity of the single-photon source and that the source brightness increases with increasing pulse width. More importantly, in contrast to the photon antibunching induced in coupled cavity systems [22], in a certain parameter regime (namely, with zero detuning), oscillations in  $g^{(2)}(\tau)$  are fully suppressed, and therefore our model is naturally suitable to serve as a pulse-regulated single-photon source with high purity under pulsed excitation.

We consider a model consisting of a driven dissipative nonlinear nanocavity (i.e., a photonic crystal cavity or a micro-ring/disk), as shown schematically in Fig. 1(a). The fundamental mode and the second-harmonic mode are spatially overlapping in the same nanocavity at resonance frequencies  $\omega_a$  and  $\omega_b = 2\omega_a$ , respectively. The two modes are coupled through  $\chi^{(2)}$  nonlinearity that mediates the conversion of one photon in mode  $\hat{b}$  to two photons in mode  $\hat{a}$ , and vice versa. The fundamental mode  $\hat{a}$  is driven by a weak driving light with strength  $E$  and frequency  $\omega_d$ . The second-harmonic mode  $\hat{b}$  is driven by a strong pump light with strength  $F$  and frequency  $2\omega_d$ . In the rotating frame of the driving and pump lights, the Hamiltonian of the system is (with  $\hbar = 1$ )

$$\hat{H} = \Delta\hat{a}^\dagger\hat{a} + 2\Delta\hat{b}^\dagger\hat{b} + \chi(\hat{b}\hat{a}^{2\dagger} + \hat{b}^\dagger\hat{a}^2) + E(\hat{a}^\dagger + \hat{a}) + F(e^{-i\theta_0}\hat{b}^\dagger + e^{i\theta_0}\hat{b}), \quad (1)$$

where  $\Delta = \omega_a - \omega_d$  is the detuning between the fundamental mode and the driving light,  $\chi$  is the parametric gain, and  $\theta_0$  is the phase difference between the driving light and the pump light, which can be adjusted by a movable mirror outside the nanocavity. In contrast to the system considered in Ref. [25], we here assume the pump light is very strong and the depletion by the fundamental mode is negligible, hence the second-harmonic mode can be approximately expressed as  $\hat{b} \simeq F/\sqrt{4\Delta^2 + \gamma^2/4} e^{-i\theta}$  with  $\theta = \tan^{-1}[\gamma/(4\Delta)] - \theta_0$ , where we have introduced the decay rate of second-harmonic mode  $\gamma$ . Substituting this expression into Hamiltonian (1), we have

$$\hat{H} = \Delta\hat{a}^\dagger\hat{a} + E(\hat{a}^\dagger + \hat{a}) + U(e^{i\theta}\hat{a}^{2\dagger} + e^{-i\theta}\hat{a}^2), \quad (2)$$

where  $U = F\chi/\sqrt{4\Delta^2 + \gamma^2/4}$  is the effective parametric gain. Note that for a coherent driving field,  $E$  is constant, while for pulsed driving,  $E$  is time-dependent. The Hamiltonian (2) describes an optical cavity excited by both parametric and coherent driving fields, which is the starting point for the following calculation.

According to Ref. [26], in the limit of weak driving  $E \ll \kappa$  and low parametric gain  $U \ll \kappa$  (far below the threshold for parametric oscillation), one can obtain the optimum condition for strong antibunching:  $E^2 = U\sqrt{\Delta^2 + \kappa^2/4}$  and  $\theta = \tan^{-1}(\kappa/2\Delta)$ . The strong antibunching comes from the quantum destructive interference between two different two-photon events: one coming from coherent driving,  $|0\rangle \xrightarrow{E} |1\rangle \xrightarrow{E} |2\rangle$ , and the other from parametric down-conversion,  $|0\rangle \xrightarrow{U} |2\rangle$ . Such a system can be viewed as a stochastic single-photon source under CW driving. However, for a deterministic single-photon source, one requires single-photon emission at deter-

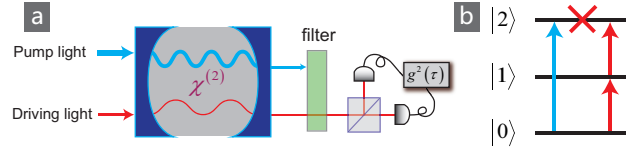


**Fig. 1.** (a) Scheme for single-photon generation in a nonlinear-nanocavity-based optical parametric amplifier driven by a strong harmonic pump and a weak fundamental driving field. Emitted photons from the right channel can be collected and analyzed by a photon counter. (b) Energy level diagram. The quantum destructive interference between different two-photon events from coherent excitation and parametric down-conversion leads to a vanishing probability of the two-photon state.

mined times. Therefore, in order to prepare a pulse-regulated single-photon source, our system should be operated in the pulsed regime.

Given that single-photon sources in the telecommunications band are of great interest in the context of quantum information processing on chips, the operational wavelength of the fundamental mode of the nanocavity is assumed to be  $1.5 \mu\text{m}$ . To date, various nanocavities made of noncentrosymmetric materials (e.g., GaP and GaAs) with high quality factor ( $Q = 10^5 \sim 10^6$ ) have been designed and fabricated [27]. Therefore, we can choose a nanocavity with a quality factor  $Q \sim 10^6$ , which gives a cavity-mode linewidth  $\kappa \sim 1 \text{ GHz}$ . For III-V semiconductor materials, the second-order susceptibility  $\chi^{(2)}$  is typically of the order of  $10^{-10} \text{ m/V}$ . If the nanocavity is made up of photonic crystal cavities, for an optimum geometric configuration, the realistic maximum value of the nonlinear coupling  $\chi$  can reach  $1 \text{ GHz}$ . Hence we can safely assume a suitable parametric gain  $U$  in the following study.

To study the photon statistics of the emitted field in the pulsed-driving situation, we need to analyze the second-order correlation function with delay. Using the quantum regression theorem [28], we have the time-dependent correlation function

$$g^{(2)}(\tau) = \frac{\langle \hat{a}^\dagger \hat{a}^\dagger(\tau) \hat{a}(\tau) \hat{a} \rangle}{\langle \hat{a}^\dagger \hat{a} \rangle^2} = \frac{\text{Tr} \{ \hat{a}^\dagger \hat{a} e^{\hat{L}\tau} [\hat{a} \hat{\rho}_{ss} \hat{a}^\dagger] \}}{\text{Tr} (\hat{a}^\dagger \hat{a} \hat{\rho}_{ss})^2}, \quad (3)$$

where  $\hat{\rho}_{ss}$  is the reduced density matrix for mode  $\hat{a}$  in the steady state, and the superoperator  $\hat{L}$  is defined as

$$\hat{L}\hat{\rho} = -i[H, \hat{\rho}] + \frac{\kappa}{2}\hat{D}[\hat{a}]\hat{\rho}, \quad (4)$$

with the Lindblad operator  $\hat{D}[\hat{A}]\hat{\rho} = 2\hat{A}\hat{\rho}\hat{A}^\dagger - \hat{A}^\dagger\hat{A}\hat{\rho} - \hat{\rho}\hat{A}^\dagger\hat{A}$ .

Figure 2(a) shows the second-order correlation function as a function of time delay for different detunings. One can see that for nonzero detuning, the second-order correlation function oscillates with period  $2\pi/\Delta$ , and the output light is antibunched over a time delay shorter than  $1/\Delta$ . Similar oscillatory phenomena in  $g^{(2)}(\tau)$  have been observed in other situations [6, 29]. This behavior implies that the width of the driving pulse  $\Delta t$  should be larger than  $1/\Delta$  to guarantee strong antibunching of the output light. However, in the case of zero detuning,  $g^{(2)}(\tau) < 1$  for all time delays. This suggests that the limitation

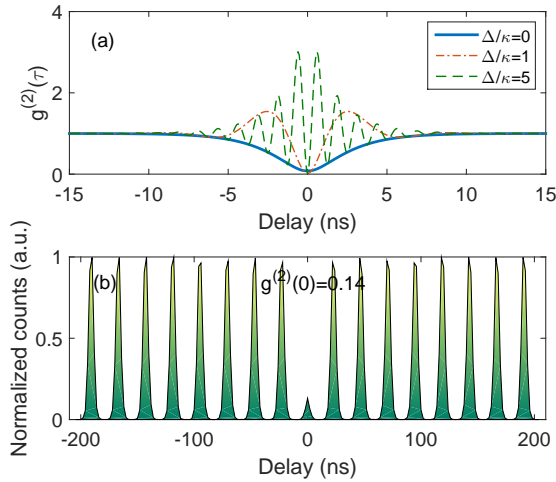


**Fig. 2.** (a) Second-order correlation function as a function of time delay  $\tau$  with different detunings  $\Delta$ . The driving strength  $E = 50$  MHz. (b) Normalized coincident counts with pulsed excitation. The equal-time second-order correlation function  $g^{(2)}(0) = 0.14$ . The width of the excitation pulse is 2 ns, the interval is 24 ns, and the maximum amplitude of the driving strength  $E_0 = 50$  MHz.

on the width of the driving pulse no longer exists in the zero-detuning case of our model. Therefore, our model is well suited for generating photon antibunching with pulsed excitation.

Next we turn to demonstrating the process of antibunching photons emitted from the nanocavity driven by a series of light pulses. In our numerical calculation, the driving field is assumed to be  $E = E_0 \exp[-(t - nt_0)^2/\Delta t^2]$ , with  $\Delta t$  being the pulse width and  $t_0$  the time at which the driving reaches its maximum value  $E_0$ . To achieve ideal antibunching in the case of pulsed excitation, the parametric gain and relative phase have to satisfy optimum conditions. Obviously, the parametric gain is also time-dependent, i.e.,  $U(t) = E^2(t)/\sqrt{\Delta^2 + \kappa^2/4}$ , which requires the pump light to have the same temporal shape as the excitation light  $E^2$ . To avoid overlapping of adjacent excitation pulses, we set the interval between them as 12 times the pulse width. Of course, there are constraints on the pulse width. For instance, the spectral width of the pulses should be smaller than the nonlinear shift of the energy levels.

To better illustrate the quantum statistics of the output light, we adopt the Monte Carlo wave-function method to simulate the stochastic evolution of the system and count the photon number from the output port [30], which closely mimics the Hanbury Brown–Twiss (HBT) experimental procedure. We extract the correlation function information from a single but sufficient long trajectory. Below, we briefly introduce the procedure involved in using the Monte Carlo wave-function method to simulate the stochastic photon emission from the nanocavity in our model.

First, we choose a pure state  $|\psi(t)\rangle$  as the system state, and then let it evolve nonunitarily for a very short but finite time interval  $\delta t$  ( $\kappa\delta t \ll 1$ ) as

$$|\tilde{\psi}(t + \delta t)\rangle = \left(1 - \frac{iH_{\text{eff}}\delta t}{\hbar}\right)|\psi(t)\rangle, \quad (5)$$

where the non-Hermitian Hamiltonian  $\hat{H}_{\text{eff}} = \hat{H} - i\hat{J}^\dagger\hat{J}/2$ , with

$\hat{J} = \sqrt{\kappa}\hat{a}$  being the jump operator. The second term in  $\hat{H}_{\text{eff}}$  is non-Hermitian, representing the dissipation induced by coupling with the environment. The norm of the evolved function wave  $\langle\tilde{\psi}(t + \delta t)|\tilde{\psi}(t + \delta t)\rangle = 1 - \delta p$  can be considered as the probability of no photon emission happened in the time interval  $\delta t$ , and  $\delta p = \delta t\langle\tilde{\psi}(t)|\hat{J}^\dagger\hat{J}|\tilde{\psi}(t)\rangle$  corresponds to the probability of a photon emission event.

Second, we decide whether an emission event occurs or not by comparing  $\delta p$  with a uniformly generated random number  $r$  ( $0 \leq r \leq 1$ ). If  $r > \delta p$ , no photon emission event occurs, and we normalize the wave function:

$$|\psi(t + \delta t)\rangle = \frac{|\tilde{\psi}(t + \delta t)\rangle}{\sqrt{1 - \delta p}}. \quad (6)$$

Otherwise, one photon is emitted, and the system state is collapsed to a new state:

$$|\psi(t + \delta t)\rangle = \frac{\hat{J}|\tilde{\psi}(t + \delta t)\rangle}{\sqrt{\delta p/\delta t}}. \quad (7)$$

The state  $|\psi(t + \delta t)\rangle$  will serve as the initial state for the next step in the iteration. By repeating this procedure, we can obtain the wave function of the system state at all times, and the system properties, including the second-order correlation function of the photons, can be evaluated based on the wave function.

We now show how to extract the correlation function from the simulated results based on the Monte Carlo wave function. Assuming a photon count taking place at time  $t$ , we cumulate the emitted photon number  $N(t, t + \tau)$  in an interval  $\Delta\tau$  at  $t + \tau$ . To achieve a balance between resolution and statistical fluctuations, the interval  $\Delta\tau$  should be carefully chosen in the calculation. We average the  $N(t, t_j)$  over all  $t$  to obtain  $\bar{N}(t, t_j) = \sum_t N(t, t_j)/N_{\text{total}}$ , where  $N_{\text{total}}$  is the total number of photons emitted during the total counting duration  $T$ . Statistically, for a sufficiently large sample, this mean value  $\bar{N}$  is closely related to the conditional probability of finding a second photon at time  $t + \tau$  provided that a first photon was detected at time  $t$ . Finally, the second-order correlation function with time delay is found as

$$g^{(2)}(\tau) = \frac{\bar{N}(t, t + \tau)}{\bar{N}(t)}, \quad (8)$$

where  $\bar{N}(t) = N_{\text{total}}\Delta\tau/T$  is the mean photon number in an interval  $\Delta\tau$  in the steady state. In the simulation, we set the total number of excitation pulses as  $10^7$ , and the width and amplitude of each excitation pulse are 2 ns and 0.05 eV, respectively. The detuning  $\Delta = 0$  and the interval between excitation pulses is 24 ns, corresponding to a 42 MHz repetition rate. Figure 2(b) shows the normalized number of counts versus the time delay. The second-order correlation function  $g^{(2)}(0) \simeq 0.14$  is calculated from the integrated number of photon counts in the zero-delay peak divided by those in its adjacent peak. In the numerical experiment, we observe a count rate of 800 000 per second, under excitation at a repetition rate of 42 MHz, which gives an overall system efficiency of 1.9%.

From a practical viewpoint, the purity and brightness of a single-photon source are two important features of merit. Here we investigate the influence of the parameters of the excitation pulse upon these features. As described in the literature, the purity is usually characterized by the zero-delay second-order correlation function  $g^{(2)}(0)$  and the brightness by the emitted

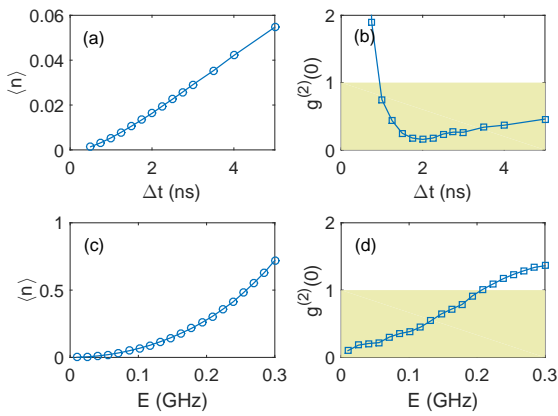


**Fig. 3.** (a) Mean photon number (brightness) and (b) equal-time second-order correlation function (purity) as functions of excitation pulse width with maximum driving strength  $E_0 = 50$  MHz. (c) Mean photon number (brightness) and (d) equal-time second-order correlation function (purity) as functions of the maximum driving strength  $E_0$  for pulse width  $\Delta t = 2$  ns.

photon number per excitation pulse  $\langle n \rangle$  [31]. Figure 3 shows numerical results for the brightness and purity as functions of the width and strength of the excitation pulse. For fixed maximum strength  $E_0 = 50$  MHz [as shown in Fig. 3(a)], the brightness increases monotonically with increasing width  $\Delta t$ . Figure 3(b) shows that  $g^{(2)}(0)$  decreases and then increases with increasing width  $\Delta t$ . The minimum value of  $g^{(2)}(0)$  can reach 0.14, corresponding to high purity of the single-photon source. The reason for this behavior is that a small temporal width of the excitation pulse corresponds to a large width in the frequency domain, and consequently most frequency components of the pulse deviate dramatically from the optimum condition, leading to an increase in the second-order correlation function. On the other hand, longer pulse excitation means an increased probability for the detector to collect two or more photons per excitation pulse, and this also increases  $g^{(2)}(0)$ . Therefore, an optimum width for the excitation pulse is helpful to achieve a minimum  $g^{(2)}(0)$ . Figures 3(c) and 3(d) illustrate that, for a fixed width of the excitation pulse  $\Delta t = 2$  ns, both brightness and  $g^{(2)}(0)$  increase monotonically as the maximum driving strength is increased. This can be attributed to an increase in the population of multiphoton states brought about by the increased driving strength.

In conclusion, we have investigated pulse-regulated integrable single-photon generation in a weak  $\chi^{(2)}$  nonlinear nanocavity and have analyzed statistical properties of the emitted photons via the Monte Carlo wave-function method. For a typical cavity mode linewidth  $\kappa \sim 1$  GHz, the maximum single-photon repetition rate reaches 42 MHz, the purity is  $\sim 0.14$ , and the efficiency is 1.9%. We have found that for fixed driving strength, there exists an optimum pulse width for achieving maximum purity and that the purity can be further improved at the cost of reduced generation efficiency by decreasing the driving strength. Our work may offer direct guidance for experimental construction of pulse-regulated single-photon sources via quantum interference.

## 1. FUNDING INFORMATION

National Natural Science Foundation of China (NSFC) (11664014, 11504145, and 11364021); Natural Science Foundation of Jiangxi Province (20161BAB201023 and 20161BAB211013).

## REFERENCES

1. C. H. Bennett, G. Brassard, C. Crepeau, R. Jozsa, A. Peres, and W. K. Wootters, *Phys. Rev. Lett.* **70**, 1895 (1993).
2. T. C. Ralph, A. G. White, W. J. Munro, and G. J. Milburn, *Phys. Rev. A* **65**, 012314 (2001).
3. X. Ding, Y. He, Z. C. Duan, N. Gregersen, M. C. Chen, S. Unsleber, S. Maier, C. Schneider, M. Kamp, S. Hofling, C.-Y. Lu, and J.-W. Pan, *Phys. Rev. Lett.* **116**, 020401 (2016).
4. M. B. Ward, O. Z. Karimov, D. C. Unitt, Z. L. Yuan, P. See, D. G. Gevaux, and A. J. Shields, *Appl. Phys. Lett.* **86**, 201111 (2005).
5. T. C. H. Liew and V. Savona, *Phys. Rev. Lett.* **104**, 183601 (2010).
6. M. Bamba, A. Imamoglu, I. Carusotto, and C. Ciuti, *Phys. Rev. A* **83**, 021802 (2011).
7. K. M. Birnbaum, A. Boca, R. Miller, A. D. Boozer, T. E. Northup, and H. J. Kimble, *Nature* **436**, 87 (2005).
8. H. Flayac and V. Savona, *Phys. Rev. A* **96**, 053810 (2017).
9. H. J. Sniijders, J. A. Frey, J. Norman, H. Flayac, V. Savona, A. C. Gosard, J. E. Bowers, M. P. van Exter, D. Bouwmeester, and W. Löffler, *Phys. Rev. Lett.* **121**, 043601 (2018).
10. C. Vaneph, A. Morvan, G. Aiello, M. Féchant, M. Aprili, J. Gabelli, and J. Estève, *Phys. Rev. Lett.* **121**, 043602 (2018).
11. Y. J. Lu and Z. Y. Ou, *Phys. Rev. Lett.* **88**, 023601 (2001).
12. T. B. Pittman, J. D. Franson, and B. C. Jacobs, *New J. Phys.* **9**, 195 (2007).
13. Y. J. Lu, L. Zhu, and Z. Y. Ou, *Phys. Rev. A* **71**, 032315 (2005).
14. M.-A. Lemonde, N. Didier, and A. A. Clerk, *Phys. Rev. A* **90**, 063824 (2014).
15. M. Li, C.-M. Zhang, Z.-Q. Yin, W. Chen, S. Wang, G.-C. Guo, and Z.-F. Han, *Opt. Lett.* **39**, 880 (2014).
16. M. Scholz, L. Koch, and O. Benson, *Phys. Rev. Lett.* **102**, 063603 (2009).
17. C. Simonneau, J. P. Debray, J. C. Harmand, P. Vidakovic, D. J. Loving, and J. A. Levenson, *Opt. Lett.* **22**, 1775 (1997).
18. Z. Yang and J. E. Sipe, *Opt. Lett.* **32**, 3296 (2007).
19. S. Mariani, A. Andronico, O. Mauguin, A. Lemaitre, I. Favero, S. Ducci, and G. Leo, *Opt. Lett.* **38**, 3965 (2013).
20. M. Davanco, J. R. Ong, A. B. Shehata, A. Tosi, I. Agha, S. Assefa, F. Xia, W. M. J. Green, S. Mookherjea, and K. Srinivasan, *Appl. Phys. Lett.* **100**, 261104 (2012).
21. L. Dusanowski, P. Holewa, A. Marynski, A. Musial, T. Heuser, N. Srocka, D. Quandt, A. Strittmatter, S. Rodt, J. Misiewicz, S. Reitzenstein, and G. Sek, *Opt. Express* **25**, 31122 (2017).
22. H. Flayac, D. Gerace, and V. Savona, *Sci. Reports* **5**, 11223 (2015).
23. A. Majumdar and D. Gerace, *Phys. Rev. B* **87**, 235319 (2013).
24. D. Gerace and V. Savona, *Phys. Rev. A* **89**, 031803 (2014).
25. Y. H. Zhou, H. Z. Shen, and X. X. Yi, *Phys. Rev. A* **92**, 023838 (2015).
26. B. Sarma and A. K. Sarma, *Phys. Rev. A* **96**, 053827 (2017).
27. B. Guha, F. Marsault, F. Cadiz, L. Morgenroth, V. Ulin, V. Berkovitz, A. Lemaitre, C. Gomez, A. Amo, S. Combric, B. Gerard, G. Leo, and I. Favero, *Optica* **4**, 218 (2017).
28. C. W. Gardiner and P. Zoller, Springer Berlin (2004).
29. G. Rempe, R. J. Thompson, R. J. Brecha, W. D. Lee, and H. J. Kimble, *Phys. Rev. Lett.* **67**, 1727 (1991).
30. R. Dum, P. Zoller, and H. Ritsch, *Phys. Rev. A* **45**, 4879 (1992).
31. N. Somaschi, V. Giesz, L. D. Santis, J. C. Loredo, M. P. Almeida, G. Hornecker, S. L. Portalupi, T. Grange, C. Anton, and J. Demory, *Nat. Photonics* **10** (2015).